Solar Energy Materials & Solar Cells 238 (2022) 111628

Contents lists available at ScienceDirect

Solar Energy Materials and Solar Cells

journal homepage: www.elsevier.com/locate/solmat

I–V-curve analysis using evolutionary algorithms: Hysteresis compensation in fast sun simulator measurements of HJT cells

David Hevisov, Kai Sporleder, Marko Turek *

Fraunhofer Center for Silicon Photovoltaics CSP, Otto-Eißfeldt-Str. 12, 06120, Halle Saale, Germany

ARTICLE INFO

Keywords:
Solar simulators
Fast current-voltage measurement
Hysteresis compensation
Evolutionary algorithms

ABSTRACT

State-of-the-art solar cell technologies, such as hetero-junction cells or PERC cells, exhibit a time-dependent deformation of their current-voltage characteristics in fast solar simulator measurements. This hysteresis effect is due to an increased internal capacitance. It manifests itself as a pronounced difference between I–V-curves depending on the measurement direction, i.e. $I_{sc} \rightarrow V_{oc}$ or $V_{oc} \rightarrow I_{sc}$. Thus, it leads to an imprecise determination of the cell performance parameters in particular at the maximum power point. In this study, an algorithm-based correction procedure for these capacitance-induced effects is presented. Using evolutionary optimization algorithms, our correction approach allows the determination of a steady-state curve together with the extraction of all cell parameters featured in a time-dependent equivalent circuit model. It can be implemented without any hardware upgrades and applied to measurement times as low as a few milliseconds. As our basic approach is entirely independent of the underlying model, it is applicable to any solar cell technology by adapting the model under consideration.

1. Introduction

The acquisition of the current-voltage (I–V) characteristic is one of the standard procedures for the characterization of solar cells. It allows easy access to various cell and performance parameters, such as the fill factor (*FF*) or the maximum power (P_{max}). Accordingly, an accurate measurement of the I–V characteristic is crucial to categorize the cells correctly in terms of their efficiency, both in research laboratories as well as in production environments. However, for inline applications, the available measurement time per cell is limited by the throughput of the production line and measurement times of significantly less than 100 ms may occur. This is especially the case, if additional non-STC measurements or electroluminescence imaging are integrated in this measurement step for improved quality assurance.

For state-of-the-art cell technologies, for instance PERC (Passivated Emitter and Rear Cell) or HJT (Heterojunction technology), this results in measurement inaccuracies due to capacity effects of the solar cells. Modern high efficiency solar cells exhibit extended minority carrier lifetimes and diffusion lengths [1,2], resulting in a significant amount of charge being stored in the quasi-neutral region of the diode [3]. Depending on the sweep direction performed during the I–V measurement, forward (from I_{sc} to V_{oc}) or reverse (from V_{oc} to I_{sc}), a charging respectively discharging of this area can be observed related to the diffusion capacitance. This capacitance causes a time-dependent distortion of the current-voltage characteristic, leading to significant deviations in the calculation of the performance parameters, in particular for measurement times well below 50 ms. Depending on whether the voltage increases or decreases with time, a reduced or additional current contribution occurs, leading to an asymmetrical splitting of the forward and reverse curve with respect to the steady-state curve, also referred to as hysteresis.

Many different techniques have been presented in the last few years aiming at the correction of these hysteresis effects. The previously developed approaches can basically be grouped into two categories: metrological solutions, such as presented in Refs. [4–8] and approaches based on physical modelling of the capacitance combined with numerical approaches, as for example in Refs. [9–14]. The authors in Refs. [4,5] utilize an adapted voltage profile to ensure that the capacitance is always charged when measuring the individual current values in order to reproduce the steady state curve. For higher capacities, however, this results in increased waiting times or only a limited number of data points can be acquired. In Ref. [6], quickly measured dark and light I–V curves are combined with the measurement of a slowly acquired dark I–V curve to calculate the illuminated steady-state curve. The very short exposure

* Corresponding author.
E-mail address: marko.turek@csp.fraunhofer.de (M. Turek).

https://doi.org/10.1016/j.solmat.2022.111628
Received 5 May 2021; Received in revised form 19 January 2022; Accepted 26 January 2022
Available online 1 February 2022

time can extend the lifespan of the light source and minimize thermal effects, nevertheless a considerable measurement time is needed to record the dark steady-state curve. The combination of dark I–V- and impedance-measurements with illuminated I–V-curves is demonstrated in Ref. [7]. In Ref. [8], a detailed analysis of the parameters defining the measurement process, such as voltage hold times or measurement delay times, is presented. An analytical model describing the temporal change in excess carrier density within the entire device and its impact on a fast I–V-curve measurement has been presented by Sinton et al. in Ref. [9]. It is argued that the diffusion capacitance is the major reason for the observed capacity effects in modern silicon solar cells. This approach has been demonstrated on a set of solar cell and module samples in Ref. [10]. A similar approach using the weighted sum of currents, as in Refs. [8,9], has been applied to the monitoring of modules in an outdoor PV system by implementing it in a low-cost electronic system [11]. As it requires the knowledge of the series resistance, which is assumed to be given by a fixed value, the error due to the uncertainty in this value is presented in Ref. [12]. The more complex case that the series resistance depends on the illumination or current, as shown in Ref. [13], is not included. These model-based numerical correction procedures, such as in Refs. [9–12], provide a correction scheme for individual measurement points of the entire I–V-curve in order to determine the steady-state curve from at least two fast I–V-measurements and require the knowledge of the series resistance. Also, the rely on the time derivatives of the measured quantities thus being sensitive to noise in the measurement data and the choice of the adequate routine for the calculation of the derivatives is critical. Finally, we would also like to mention the most straightforward method of correcting hysteresis by simply averaging the forward and reverse curves. Although the correction method based on averaging provides a sufficiently accurate determination of the performance parameters in the case of slightly pronounced hysteresis, the accuracy decreases enormously as the hysteresis effect becomes more severe.

In this work, a data analysis method based on optimization algorithms will be introduced to allow hysteresis correction using illuminated I–V characteristics. For this purpose, the free model parameters of an adapted time-dependent double diode model similar to the equivalent circuit presented in Ref. [3], are determined by an evolutionary optimization algorithm, more precisely the Differential Evolution (DE) algorithm [15]. In this way, the deviation between the model function and the experimental I–V data will be minimized. On the basis of the model function, a steady-state curve without capacitive effects can then be calculated. As the optimization algorithm includes the entire I–V-curve into the calculation and not just single measurement points, it is rather robust with respect to measurement noise. It thus enables an accurate determination of the performance parameters even for measurement times in the millisecond range. Furthermore, all cell parameters included in the model can be extracted for both I–V data with and without hysteresis effect. In addition to the established cell parameters of the double diode model, the diffusion capacitance can also be obtained from the modified double diode equation, providing an additional point of view in the characterization process.

In order to first investigate the applicability of the chosen algorithm, we have performed several benchmark tests on artificial numerical data sets for time-independent I–V-curves. We show that the DE-algorithm applied to I–V-data sets is robust and yet shows a fast convergence for a limited number of iterations. We find that typical fit results yield Root Mean Square Error (*RMSE*) values of about 10^{-6} A. In a next step, we present results on the hysteresis compensation of time-dependent numerical model data sets proving that our approach indeed allows for the reliable determination of steady-state I–V-curves with a high degree of accuracy. Third, we present our results for experimental data. In particular, we analyze measurements obtained in the range from about 800 ms down to 6 ms. Even for the fastest measurements, the steady-state fill factor can be determined with a minimal error of about $0.1\%_{\mathrm{rel}}$. Finally, we show that the extracted value for the capacitance can serve as an early indication for a solar cell degradation.

The paper is structured as follows. In Section 2, a time-dependent extension of the two-diode model is introduced. Then, in Section 3, the procedure for cell parameter extraction is presented using the DE algorithm. The results are presented in Section 4 while in Section 5 our conclusions are drawn from the results.

2. Modelling the I–V characteristics of solar cells

Our algorithm-based hysteresis compensation approach relies on the applicability of a parameterizable time-dependent model of the solar cell. However, the basic concept using the evolutionary algorithms is entirely independent of the chosen model and thus applicable to any solar cell technology. In this work, we have employed the double diode model where a current source for the photogenerated current I_{ph} is connected in parallel with two diodes $D1$ and $D2$. Additionally, a parallel (shunt) resistance R_{sh} and a series resistance R_s are included to model the most relevant electrical loss mechanisms. Therefore, the total current I is given as

$$I(U) = I_{ph} - I_{D1} - I_{D2} - I_{sh} = I_{ph} - I_{01}\left[\exp\left(\frac{e(U+IR_s)}{n_1 k_B T}\right) - 1\right] - I_{02}\left[\exp\left(\frac{e(U+IR_s)}{n_2 k_B T}\right) - 1\right] - \frac{U+IR_s}{R_{sh}} \tag{1}$$

where U is the cell voltage, I_{D1} and I_{D2} are the currents of the diffusion and recombination diode, respectively, and I_{sh} is the shunt current. I_{D1} and I_{D2} are given by the Shockley diode equation where I_{01} and I_{02} are the respective saturation currents; and n_1 and n_2 are the first and second diode ideality factors, respectively. The Boltzmann constant is denoted by k_B while e is the elementary charge and T is the temperature (see Fig. 1).

The time-dependent distortion of the current-voltage characteristics of high efficiency solar cells can be explained by the voltage-dependent cell capacitance. The total capacitance C of a solar cell is composed of the diffusion capacitance C_{diff} and the depletion layer capacitance C_{dep}. However, the latter is negligibly small in the range of the hysteresis and

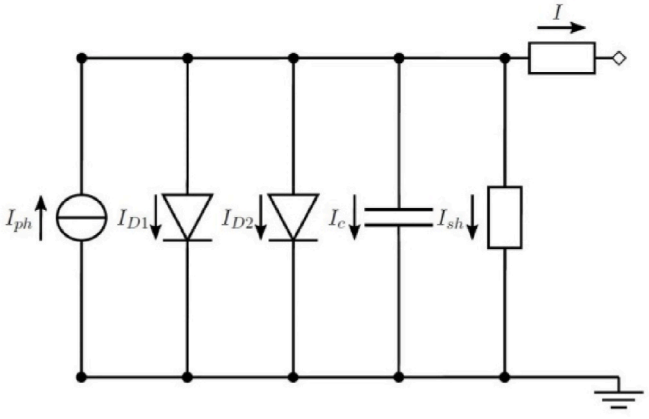

Fig. 1. Equivalent circuit of the time-dependent double diode model.

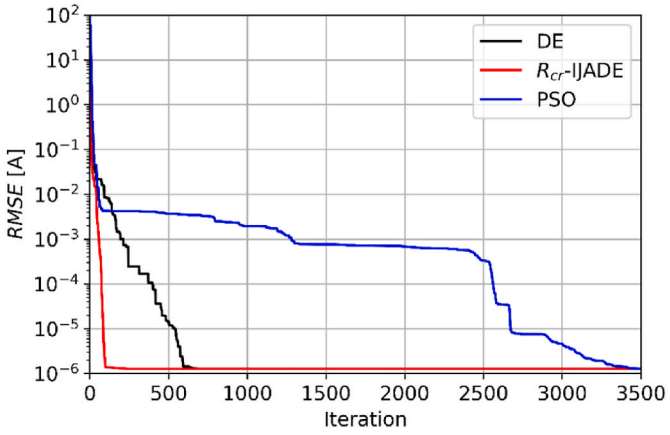

Fig. 2. Comparison of the convergence behavior: course of the *RMSE*.

is therefore not taken into account for the further calculations [3]. In order to account for the capacitance-induced effects, an additional capacitor is thus added to the equivalent circuit of the double diode model, see Fig. 2, analogous to the equivalent circuit presented in Ref. [3].

Considering the time-dependency, the total current $I(t)$ now yields

$$I(t) = I_{ph} - I_{D1}(t) - I_{D2}(t) - I_{sh}(t) - I_c(t) \tag{2}$$

where $I_c(t)$ is the capacitor current.

Assuming that the voltage dependency of the diffusion capacitance C satisfies the following exponential relationship [3,15,16].

$$C = C_0 \cdot \exp\left(U_c(t) \cdot \frac{ae}{k_B T}\right) \tag{3}$$

where C_0 is the diffusion capacitance at $U_c = 0$ and a is a fit parameter, the following differential equation is obtained:

$$CR_s\left(\frac{ae}{k_B T}U_c + 1\right)\left(\frac{dI}{dt} + \frac{1}{R_s}\frac{dU}{dt}\right) + I(t) = I_{ph} - I_{D1}(t) - I_{D2}(t) - I_{sh}(t). \tag{4}$$

Solving this equation for a known voltage profile $U(t)$, the time-dependent current $I(t)$ can thus be calculated numerically leading to a new model function describing the time-dependent I–V characteristics of high efficiency solar cells.

3. Cell parameter extraction USING EVOLUTIONARY ALGORITHMS

The model functions introduced in Section 2 feature a number of different free model parameters. For the case of the time-dependent double diode model (Eq. (4)), one can define a parameter vector as:

$$\vec{x} = \left(I_{ph}, I_{01}, I_{02}, n_1, n_2, R_s, R_{sh}, a, C_0\right). \tag{5}$$

To find a model function that fits a given set of I–V data as accurately as possible, it is necessary to determine the free model parameters $\vec{x}$ so that the deviation between the data and the model function will be minimized. In our approach, this is realized by means of optimization algorithms. To this end, an objective function $F(\vec{x})$ must be defined, which is minimized in the course of the optimization process. One possible objective function is the Root Mean Square Error (*RMSE*) (Eq. (6)), which is also used in numerous similar works [18–22].

$$RMSE(\vec{x}) = \sqrt{\frac{1}{N}\sum_{k=1}^{N}\left(I_k - I_{mod,k}(\vec{x})\right)^2} \tag{6}$$

where $|I_k - I_{mod,k}|$ is the vertical distance between a current value I_k of the I–V characteristic to be fitted and a corresponding current $I_{mod,k}$ of the model function. N denotes the total number of data points of the I–V curve. In the case of the double diode model, Eq. (1), by using the known current values I_k, the implicit model function $I_{mod,k} = f(U_k, I_{mod,k})$ can be approximated by an explicit representation $I_{mod,k} = f(U_k, I_k)$, eliminating the need to solve the equation numerically. Such an approach is also possible in the case of the time-dependent double diode model (Eq. (4)). However, this leads to a mathematical expression whose numerical value depends heavily on the interpolation method, e.g. splines, being used.

For the analysis of numerical data, the vertical distance definition in Eq. (6) is sufficient, since it can be assumed that the I–V curves being fitted do not exhibit any measurement error. Considering experimental I–V data, a measurement uncertainty must generally be anticipated. In the area of larger slopes, i.e. close to V_{oc}, a minor error in the voltage values already leads to substantial errors when determining the vertical distance in the I-direction. This effect can be minimized by introducing an orthogonal distance definition instead of Eq. (6) by

$$RMSE_{orth}(\vec{x}) = \sqrt{\frac{1}{N}\sum_{k=1}^{N}\frac{\left(M_{I,k} - P_{I,k}\right)^2}{{I_{sc}}^2} + \frac{\left(M_{V,k} - P_{V,k}\right)^2}{{V_{oc}}^2}} \tag{7}$$

where $M_k = (M_{I,k}, M_{V,k})$ is the pair of current-voltage-values obtained by the model function at which the Euclidean distance to a point $P_k = (P_{I,k}, P_{V,k})$ of the I–V characteristic to be fitted is minimal. In order to obtain a dimensionless quantity, a normalization is applied with regard to I_{sc} and V_{oc} in the current and voltage dimension, respectively.

To find the set of model parameters $\vec{x}$ so that the error is minimized, we have investigated the Differential Evolution (DE) algorithm [15] which is an evolutionary optimization algorithm inspired by natural selection. The DE algorithm is mainly based on the four steps initialization, mutation, crossover and selection. At first, a random population consisting of n solution vectors $\vec{x}_i \in \mathbb{R}^d$ is initialized. Then, a mutation vector $\vec{m}_i$ is created for each solution vector $\vec{x}_i$ using the mutation operator. Subsequently, components of $\vec{x}_i$ and $\vec{m}_i$ are randomly selected to generate the trial vectors $\vec{t}_i$. In the last operator of the DE, the selection, the solution vectors $\vec{x}_i$ and $\vec{t}_i$ are now compared in a pairwise manner, whereby whichever solution vector yields the smaller value for the objective function F is taken over into the next generation $\vec{y}_i$. Setting $\vec{y}_i \rightarrow \vec{x}_i$ the DE algorithm can proceed to the next iteration until a termination criterion is met. There are many different variations of the DE algorithm, whereby in this particular case, following the nomenclature of the original paper [15], the "DE/rand-to-best/1/bin" strategy is considered as presented in Ref. [19].

4. Results

First, we use benchmark tests to quantify the errors of our implemented algorithmic approach when applied to time-independent numerical I–V-data sets. Using these results, we can define the number of initial solution vectors (swarm or population size) and the number of iterations required to obtained reliable results for the model parameters. Having identified the DE algorithm as being robust and accurate at the same time, it is applied to data sets of time-dependent data showing that our concept leads to accurate steady-state I–V curves even for very short measurement times. We then apply the optimized algorithms to experimental data finding fill factor deviations of the extracted I–V-curves being as low as $0.1\%_{rel}$. Finally, we show that the extraction of the capacitance as an additional parameter can serve as an early indication of a solar cell degradation.

4.1. Benchmark tests

In order to select a suitable optimization algorithm for hysteresis compensation, the DE algorithm [15], the R_{cr}-IJADE algorithm [19] and

the Particle Swarm Optimization [23] (PSO) are compared. They all achieved promising results in cell parameter extraction for the time-independent case [16–22]. As the relevant criteria, we analyze their effectiveness, accuracy and stability. To this end, a numerically generated I–V data set based on Eq. (1) with randomly selected cell parameters $I_{ph} = 9.37$ A, $I_{01} = 1.41{\cdot}10^{-8}$ A, $I_{02} = 4.25{\cdot}\ 10^{-7}$ A, $R_s = 0.0035\ \Omega$, $R_{sh} = 97.3\ \Omega$, $n_1 = 1.62$, $n_2 = 1.60$ is evaluated. For better comparability, 120 solution vectors $\vec{x}_i$ are used for all three algorithms. The parameters of the DE algorithm, i.e. F and CR, are chosen to be 0.9 each. As proposed in Ref. [19], the parameters of the R_{cr}-IJADE algorithm read as follows: $\mu_{cr} = \mu_F = 0.5$, $c = 0.1$ and $p = 0.05$. For the PSO algorithm according to Ref. [20], the learning factors are set to $c_1 = c_2 = 2$ and the inertia weight w is linearly decreasing from 0.9 to 0.4. The search intervals are set to $I_{ph} \in [9, 10]$, $I_{01} \in [0, 10^{-6}]$, $I_{02} \in [0, 10^{-6}]$, $R_s \in [0, 0.5]$, $R_{sh} \in [0, 1000]$, $n_1 \in [1, 2]$ and $n_2 \in [1, 2]$ for all three algorithms. To compare the effectiveness of the individual iterations, Fig. 3 shows the *RMSE* in dependence on the number of iterations for all algorithms under consideration.

With approximately 200 iterations, the R_{cr}-IJADE algorithm requires the lowest number of iterations to reach the minimum *RMSE* value of $1.28{\cdot}10^{-6}$ A. In contrast, the DE and PSO algorithm take about 700 and 3400 iterations, respectively, to reach the minimum error. Considering the required computing time per iteration, the R_{cr}-IJADE algorithm converges about two times and eight times faster than the DE and PSO algorithm, respectively. Hence, the R_{cr}-IJADE minimizes the objective function most effectively for the dataset in question.

To evaluate the convergence stability of the algorithms, the mean *RMSE* from 50 runs is determined for the same numerical data set, varying the number of iterations and solution vectors, see Fig. 3.

For the DE algorithm (a), the minimum error value (dark green) can be stably reproduced almost independently of the number of solution vectors through an increase of the iteration count. Vice versa, with the R_{cr}-IJADE algorithm (b), the minimum error value can be reliably achieved by a higher number of solution vectors, almost independently of the number of iterations. Using the PSO algorithm (c), the minimum *RMSE* can only be reached by a significantly increased number of iterations. Since the DE algorithm produces the lowest average error value, it minimizes the error function most consistently in the parameter range considered here. As the DE algorithm provides the most stable results together with an acceptable convergence speed, it was selected for the subsequent hysteresis correction.

4.2. Hysteresis compensation

As described earlier in Section 2, hysteresis can be modeled by introducing an additional capacitor in the equivalent circuit of the double diode model. By utilizing the time-dependent double diode model (Eq. (4)) as a new model function, the cell parameters of hysteresis data can now be determined analogously to the time-independent case, as in Section 4.1. Compared to the time-independent case, however, multiple I–V characteristics are now required for the fitting of hysteresis data in order to guarantee an unambiguous determination of the capacitance C_0, which decisively influences the degree of splitting for hysteresis and is therefore essential for the calculation of the steady-state curve.

4.2.1. Numerical I–V data

The hysteresis correction is first to be carried out on numerically generated data in order to validate that an explicit determination of the capacitance is possible on the basis of two I–V curves, more precisely a forward and a reverse curve. Using the time-dependent model function (Eq. (4)), 25 I–V data sets with randomly selected model parameters ($I_{ph} \in [9\ \text{A},\ 10\ \text{A}]$, $I_{01} \in [10^{-12}\ \text{A}, 10^{-10}\ \text{A}]$, $I_{02} \in [10^{-8}\ \text{A}, 10^{-6}\ \text{A}]$, $R_s \in [0.001\ \Omega,\ 0.01\ \Omega]$, $R_{sh} \in [1\ \Omega, 20\ \Omega]$, $n_1 \in [1, 1.4]$, $n_2 \in [1.6, 2]$, $C_0 \in [10^{-10}\ \text{F}, 10^{-9}\ \text{F}]$ and $a = 0.5$) are generated for a linearly increasing (U_{for}) and decreasing (U_{rev}) voltage ramp with a total time of 5 ms per voltage sweep, where the derivatives $\dot{U}_{for}$ and $\dot{U}_{rev}$ are thus 160 Vs^{-1} and $-160\ \text{Vs}^{-1}$, respectively. The differential equation (Eq. (4)) is solved using the Python package SciPy. Since no explicit initial conditions are known for the randomly chosen cell parameters, the initial conditions $I_{for}(t = 0) = I_{0,for}$ and $I_{rev}(t = 0) = I_{0,rev}$ are set to the arbitrary values $I_{0,for} = I_{ph}$ and $I_{0,rev} = I_{for}(t = 5\ \text{ms})$ when generating the hysteresis data. The cell parameter extraction is performed with 50 solution vectors and 1500 iterations using the DE algorithm, where the search intervals are $I_{ph} \in [8\ \text{A}, 11\ \text{A}]$, $I_{01} \in [0\ \text{A}, 10^{-8}\ \text{A}]$, $I_{02} \in [0\ \text{A}, 10^{-4}\ \text{A}]$, $R_s \in [0\ \Omega, 0.1\ \Omega]$, $R_{sh} \in [0\ \Omega, 25\ \Omega]$, $n_1 \in [0.5, 2.5]$, $n_2 \in [0.5, 2.5]$, $C_0 \in$

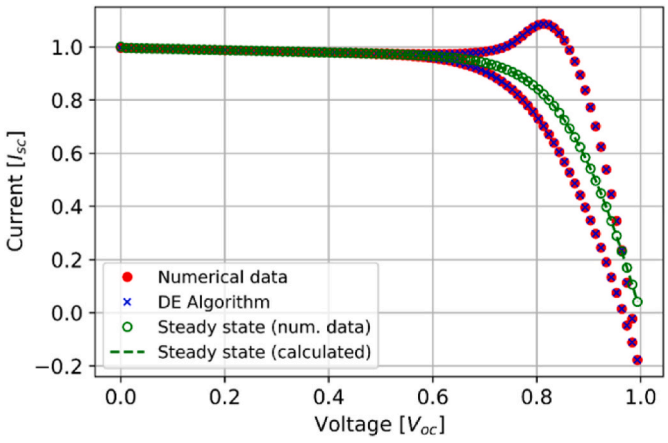

Fig. 4. Exemplary fitting of numerical hysteresis data and calculation of the steady-state curve.

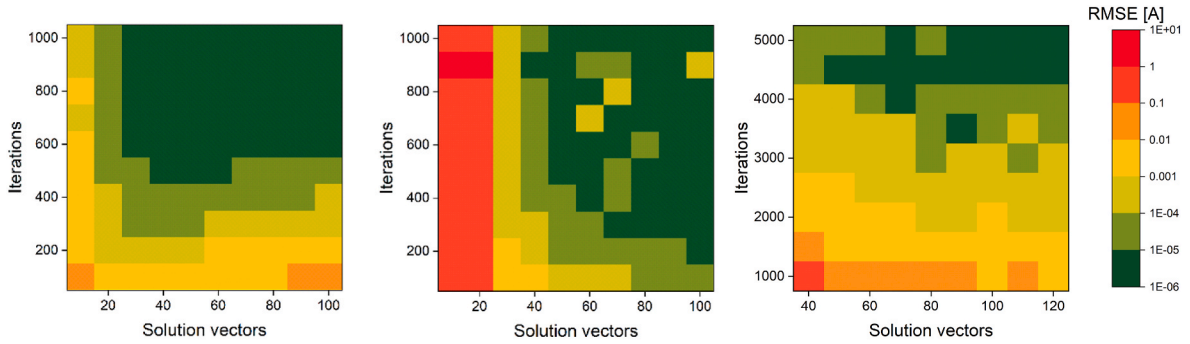

Fig. 3. Mean RMSE from 50 runs for DE (a), R_{cr}-IJADE (b) and PSO (c).

$[0\ \mathrm{F}, 10^{-7}\ \mathrm{F}]$ and $a \in [0,1]$. Whereby, for a single data set the summed *RMSE* of the forward and reverse curves is considered as the objective function.

The capacitance C_0 can be determined for the 25 numerically generated hysteresis data sets with a mean deviation of $(0.2 \pm 0.2)\%$. Thus, it can be shown that for a numerical data set consisting of at least two I–V characteristics (forward and reverse), an unambiguous determination of the diffusion capacitance is possible in the framework of the time-dependent double diode model. Fig. 4 shows an exemplary fitting of numerically generated hysteresis data for the input parameters $I_{ph} = \mathrm{A}$, $I_{01} = 6.17 \cdot 10^{-11}\ \mathrm{A}$, $I_{02} = 8.96 \cdot 10^{-7}\ \mathrm{A}$, $R_s = 0.0072\ \Omega$, $R_{sh} = 1.95\ \Omega$, $n_1 = 1.34$, $n_2 = 1.95$, $a = 0.5$ and $C_0 = 8.81 \cdot 10^{-10}\ \mathrm{F}$.

As already indicated by the low mean *RMSE* value, the calculated points of the model function show a high agreement with the numerically generated hysteresis data. Furthermore, the steady-state curve can also be reproduced with a high degree of accuracy. For the hysteresis correction, the differential equation (Eq. (4)) is solved again in the limit $C_0 \to 0$ for the extracted parameter set $\vec{x} = (I_{ph}, I_{01}, I_{02}, R_s, R_{sh}, n_1, n_2, a, C_0)$, resulting in a steady-state curve without capacitive effects. At this point, it should be noted that due to the arbitrarily set initial conditions, the steady-state curve, in contrast to experimental data, does not necessarily lie exactly between the forward and reverse curve, especially in the area around V_{oc}.

4.2.2. Experimental I–V data

The experimental hysteresis data was acquired for a heterojunction solar cell using two separate Keithley source-meters, where one of the devices was used for setting the voltage ramp and measuring the output current while the second device simultaneously measured the applied voltage. The illuminated I–V curves were recorded under standard test conditions using a SINUS-220 LED solar simulator. Whereby, the measurement time per sweep direction was varied from 5.6 ms to 794.3 ms, where 794.3 ms is referred to as the steady-state case. For the determination of the model parameters, the DE algorithm is applied with 50 solution vectors and 1500 iterations, using the orthogonal error definition given by Eq. (7). The search intervals are set to $I_{ph} \in [0\ \mathrm{A}, 10\ \mathrm{A}]$, $I_{01} \in [0\ \mathrm{A}, 10^{-6}\ \mathrm{A}]$, $I_{02} \in [0\ \mathrm{A}, 10^{-6}\ \mathrm{A}]$, $R_s \in [0\ \Omega, 0.1\ \Omega]$, $R_{sh} \in [0\ \Omega, 10^{10}\ \Omega]$, $n_1 \in [1, 2.5]$, $n_2 \in [1, 2.5]$, $C_0 \in [0\ \mathrm{F}, 10^{-6}\ \mathrm{F}]$ and $a \in [0,1]$. Generally, a linear voltage profile $U(t)$ can no longer be assumed for experimental data, therefore a cubic spline fit is implemented for the calculation of the time derivatives $\dot{U}(t)$. As an example, Fig. 5 shows the fit of experimental hysteresis data at a measurement time of 9.6 ms.

The calculated model points are in good agreement with the experimental I–V data and thus the real steady-state curve can also be predicted with good accuracy. The fill factor FF and maximal power P_{max} can be calculated with a deviation of about 0.1 $\%_{rel}$ and 1.4 $\%_{rel}$, respectively. Nevertheless, slight deviations can be seen, especially in the range around $0.7 \cdot V_{oc}$, which can likely be attributed to an insufficient number of measurement points. Further improvement of the accuracy could be achieved by more suitable optimization algorithms. Also, an adjustment of the physical model, e.g. including inductive effects as in Ref. [24], could allow for a more accurate fitting and calculation of the steady-state curve.

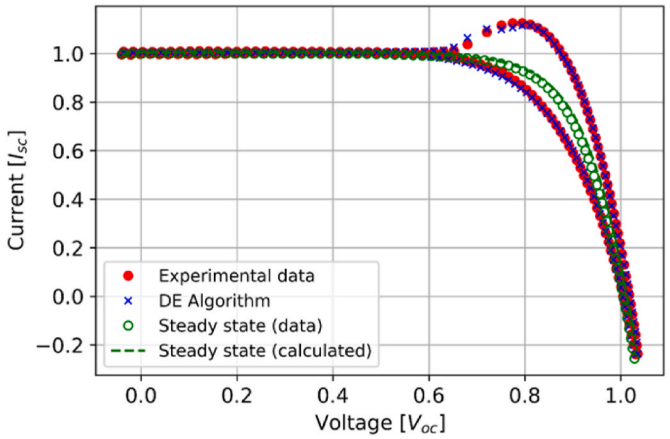

Fig. 5. Exemplary fitting of experimental hysteresis data obtained in 9.6 ms measurement time and calculation of the corresponding steady-state curve.

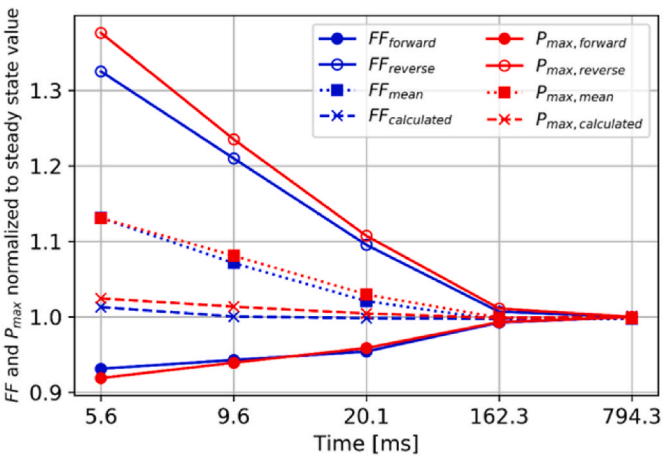

Fig. 6. Deviation in the determination of *FF* and P_{max} with respect to the steady-state values.

For the entire range of analyzed measurement times, the deviation in *FF* and P_{max} after hysteresis correction can be seen in Fig. 6 in comparison with uncorrected hysteresis data and after averaging.

Compared to uncorrected hysteresis data (solid line) or the simple averaging procedure (dotted line), the application of the DE algorithm (dashed line) yields a significantly higher accuracy in the determination of performance parameters for all measurement times under consideration. Only a slight increase of the error is observed with a progressive reduction of the measuring time down to 5.6 ms.

Finally, the hysteresis data of an artificially degraded HJT cell is evaluated, with hysteresis curves being analyzed before and after a heat treatment at 200 °C. As the HJT-technology is susceptible to high-temperature degradation, a significant power loss is expected. The measurement time in our analysis is set to 20 ms. The extracted cell capacitance C_0 and the calculated P_{max} after hysteresis compensation can be seen in Fig. 7.

The power loss can be quantified using the correction method based on optimization algorithms. More interestingly, a significant reduction

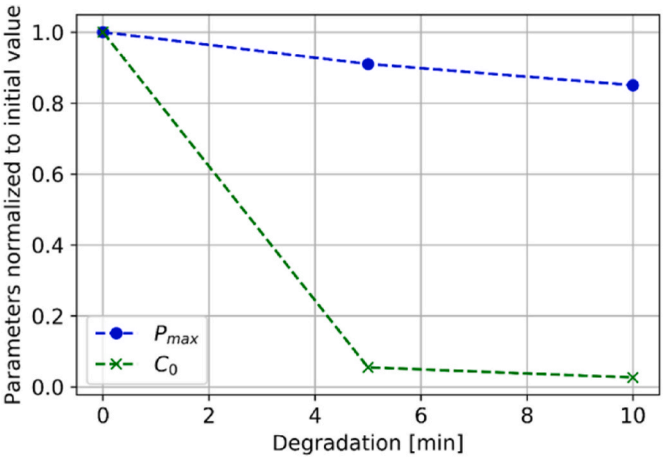

Fig. 7. Extracted cell parameters P_{max} and C_0 for different degradation levels.

of the cell capacity can be observed. Accordingly, the determination of the capacity based on fast I–V-measurements can directly serve for an early degradation detection.

5. Conclusions

In this work, a correction method for the hysteresis of current-voltage curves in fast sun simulator measurements is introduced. First, we have identified an optimal algorithm by benchmark testing several versions of evolutionary algorithms with respect to convergence speed and stability. The differential evolution (DE) algorithm turns out to be most suited for our application. Then, we have shown that the extension to a time-dependent solar cell model including a capacitance also leads to stable fit results for the corresponding steady state curve and the extracted parameters. In a third step, we have applied the optimized DE algorithm to experimental data given by I–V-curves with measurement times between about 6 ms and 800 ms. As a result, we could obtain a steady state curve which shows only minor deviations from the curve obtained for long measurement times. Finally, an example where the parameter for the capacitance is a clear indication for a cell degradation induced by thermal stress is shown.

Our approach is based on evolutionary optimization algorithms and allows an accurate determination of cell performance parameters even for very short measurement times. Since the presented hysteresis compensation method is model based, all cell parameters included in the underlying physical model can be determined for cells with and without hysteresis. As a result, we find steady state fill factors from fast-I-V data, which are most influenced by the hysteresis effects, with a minimal error of about $0.1\%_{rel}$. In addition to the parameters of the time-independent double diode model, i.e. the diffusion capacitance, can also be obtained. We have demonstrated, that this capacitance parameter provides further insight for analyzing physically relevant processes, such as degradation.

Since the data acquisition itself is not modified, no additional hardware components or measurements, as for example in the approach described in Ref. [7], are needed. However, the quality of the results obtained by using the evolutionary algorithms clearly depends on the applicability of the equivalent electrical circuit model that is employed. Also, from the perspective of gaining more physical insights, for example into material properties, the approach presented in Ref. [8] is more suitable as it is based on the physical origin of the excess charge carriers and their influence on the capacitive effects. On the other hand, our approach is based on a simultaneous analysis of all measurement points, i.e. the entire I–V-curve. This is in contrast to the method developed in Ref. [8] and applied in Refs. [9–12] which relies on the analysis of individual currents for given voltage. By considering the entire I–V-curve in one analysis step using an evolutionary algorithm, the resulting parameters are more robust with respect to measurement noise of individual measurements. Also, our approach does not require the predetermination of certain cell parameters, such as the series resistance which is crucial to the calculations as in Ref. [8]. Finally, since the evolutionary algorithms are rather universally applicable, our method is not limited to the described two diode model but can be extended to other models, e.g. for tandem solar cells, as well.

CRediT authorship contribution statement

Marko Turek: Writing – review & editing, Conceptualization.

Declaration of competing interest

The authors declare that they have no known competing financial interests or personal relationships that could have appeared to influence the work reported in this paper.

Acknowledgments

The authors thank the German Federal Ministry of Education and Research and the German Federal Ministry for Economic Affairs and Energy for financial support of the project “HJT4.0" (project no. 0324172B) and “Hossa” (project no. 03EE1014A).

References

[1] S. Zhao, Q. Qiao, S. Zhang, J. Jingjia, Z. Shi, G. Li, Rear passivation of commercial multi-crystalline PERC solar cell by PECVD Al2O3, Appl. Surf. Sci. 290 (2014) 66–70.
[2] A. Pivrikas, H. Neugebauer, N.S. Sariciftci, Charge carrier lifetime and recombination in bulk heterojunction solar cells, IEEE J. Sel. Top. Quant. Electron. 16.6 (2010) 1746–1758.
[3] G. Friesen, H.A. Ossenbrink, Capacitance effects in high-efficiency cells, Sol. Energy Mater. Sol. Cell. 48.1 (1997) 77–83.
[4] C. Monokroussos, D. Etienne, K. Morita, C. Dreier, U. Therhaag, W. Herrmann, Accurate power measurements of high capacitance PV modules with short pulse simulators in a single flash, in: Proc. 27th European Photovoltaic Solar Energy Conference, 2012, pp. 3687–3692.
[5] N. Ferretti, Y. Pelet, J. Berghold, V. Fakhfouri, P. Grunow, Performance testing of high-efficient PV modules using single 10 ms flash pulses, in: Proc. 28th European Photovoltaic Solar Energy Conference, 2013, pp. 3184–3187.
[6] H. Kojima, K. Iwamoto, A. Shimono, J. Abe, Y. Hishikawa, Accurate and rapid measurement of high-capacitance PV cells and modules using a single short pulse light, in: IEEE 40th Photovoltaic Specialist Conference, 2014, pp. 1896–1898.
[7] A.S. Eeles, R. Gottschalg, T.R. Betts, Optimising I-V measurements of high capacitance modules using dark impedance measurements, in: 2016 IEEE 43rd Photovoltaic Specialists Conference (PVSC), 2016, pp. 3693–3697, https://doi.org/10.1109/PVSC.2016.7750366.
[8] Qi Gao, Yating Zhang, Youlin Yu, Fanying Meng, Zhengxin Liu, Effects of I–V measurement parameters on the hysteresis effect and optimization in high-capacitance PV module testing, Photovolt. IEEE J. 8 (3) (2018) 710–718.
[9] R.A. Sinton, H.W. Wilterdink, A.L. Blum, Assessing transient measurement errors for high-efficiency silicon solar cells and modules, in: IEEE Journal of Photovoltaics, vol. 7, Nov. 2017, pp. 1591–1595, https://doi.org/10.1109/JPHOTOV.2017.2753200, 6.
[10] Adrienne L. Blum, Ronald A. Sinton, Harrison W. Wilterdink, Determining the accuracy of solar cell and module measurements on high-capacitance devices, in: Photovoltaic Energy Conversion (WCPEC) 2018 IEEE 7th World Conference on, 2018, pp. 3603–3606.
[11] Eneko Ortega, Gerardo Aranguren, Juan Carlos Jimeno, Photovoltaic modules self testing using M3S in an outdoor system, in: Photovoltaic Specialists Conference (PVSC) 2020 47th IEEE, 2020, pp. 1035–1041.
[12] H. Vahlman, J. Lipping, J. Hyvärinen, A. Tolvanen, S. Hyvärinen, Capacitive effects in high-efficiency solar cells during IV curve measurement: considerations on error of correction and extraction of minority carrier lifetime, in: Proc. 35th European Photovoltaic Solar Energy Conference, 2018, pp. 254–261.
[13] M. Turek, Current and illumination dependent series resistance of solar cells, J. Appl. Phys. 115 (2014) 144503, https://doi.org/10.1063/1.4871017.
[14] K. Ramspeck, S. Schenk, L. Komp, A. Metz, M. Meixner, Accurate efficiency measurements on very high efficiency silicon solar cells using pulsed light sources, in: Proc. 29th European Photovoltaic Solar Energy Conference, 2014, pp. 1253–1256.
[15] R. Storn, K. Price, Differential evolution – a simple and efficient heuristic for global optimization over continuous spaces, J. Global Optim. 11 (1997) 341–359.
[16] S.K. Sharma, D. Pavithra, G. Sivakumar, N. Srinivasamurthy, B.L. Agrawal, Determination of solar cell diffusion capacitance and its dependence on temperature and 1 MeV electron fluence level, Sol. Energy Mater. Sol. Cell. 26.3 (1992) 169–179.
[17] J.E. Mahan, D.L. Barnes, Depletion layer effects in the open-circuit- voltagedecay lifetime measurement, Solid State Electron. 24.10 (1981) 989–994.
[18] K. Ishaque, Z. Salam, S. Mekhilef, A. Shamsudin, Parameter extraction of solar photovoltaic modules using penalty-based differential evolution, Appl. Energy 99 (2012) 297–308.
[19] W. Gong, Z. Cai, Parameter extraction of solar cell models using repaired adaptive differential evolution, Sol. Energy 94 (2013) 209–220.
[20] M. Ye, X. Wang, Y. Xu, Parameter extraction of solar cells using particle swarm optimization, J. Appl. Phys. 105 (2009), 094502.
[21] K. Ishaque, Z. Salam, H. Taheri, A. Shamsudin, A critical evaluation of EA computational methods for Photovoltaic cell parameter extraction based on two diode model, Sol. Energy 85 (2011) 1768–1779.
[22] X. Yuan, Y. Xiang, Y. He, Parameter extraction of solar cell models using mutative-scale parallel chaos optimization algorithm, Sol. Energy 108 (2014) 238–251.
[23] J. Kennedy, R. Eberhart, Particle swarm optimization, in: Proc. International Conference on Neural Networks 4, 1995, pp. 1942–1948.
[24] S. Winter, J. Metzdorf, Correction procedures for the flasher calibration of PV devices resulting in reduced restrictions and uncertainties, in: Proc. 2nd World Photovoltaic Solar Energy Conference, 1998, pp. 2312–2315.